© 2020 Aaron Douglas Anderson

TESTBED DEVELOPMENT AND EXPERIMENTAL VALIDATION OF A HIGH-POWER SLOTLESS STATOR

BY

AARON DOUGLAS ANDERSON

THESIS

Submitted in partial fulfillment of the requirements
for the degree of Master of Science in Electrical and Computer Engineering
in the Graduate College of the
University of Illinois at Urbana-Champaign, 2020

Urbana, Illinois

Adviser:

Associate Professor Kiruba Sivasubramaniam Haran

ABSTRACT

This thesis presents work evaluating the performance of components of a novel high-specific-power permanent magnet synchronous machine (PMSM) for electric aircraft propulsion. An important thrust in current aerospace research is aircraft electrification, including propulsion system electrification. For an electrified propulsion system to provide net benefit over conventional propulsion, the electrical systems must meet high specific power, power density, and efficiency standards.

This thesis presents experimental validation of components of a megawatt scale permanent magnet synchronous motor targeting power density of 13 kW/kg and 96% efficiency. This experimental validation demonstrates that it is possible to build a stator appropriate for this application. The results closely match the FEA analysis and increase confidence that the final motor will be capable of meeting the design requirements. The results also highlight the importance of tight manufacturing tolerances to minimize circulating currents and associated losses.

In addition, this thesis describes work on testbed development. Specifically, the thesis discusses how to determine effective winding and resistor combinations to allow for testing the machine as a generator across a wide range of operating conditions with limited components.

ACKNOWLEDGMENTS

I could not have completed this work without support from my family who have encouraged learning from the very beginning. Along the way, numerous other educators and friends have taught me and inspired me to keep learning. For the past three years, my adviser, Dr. Kiruba Haran, and the whole Haran research group have taught me a great deal by sharing their knowledge and experience with me. Thank you.

This research would not be possible without financial support from the National Aeronautics and Space Administration, the Grainger Center for Electric Machinery and Electromechanics, and the Center for Power Optimization of Electro-Thermal Systems.

Portions of this thesis were previously published in Anderson et al., "Experimental validation of a high-power slotless stator," 2019 IEEE International Electric Machines & Drives Conference, and are used here with permission.

TABLE OF CONTENTS

LIST OF TABLES

LIST OF FIGURES

CHAPTER 1

INTRODUCTION

In recent years there has been increasing interest in aircraft electrification, including propulsion system electrification [1]. For electrified propulsion to be practical, high specific power and efficiency targets must be met [2]. To this end, a high-speed, high-frequency, air-core, permanent magnet machine with an outer rotor has previously been proposed [3], and Fig. 1.1 shows a cutaway diagram of that design. Various components of that motor have been built and tested, and results are reported in other publications [4, 5, 6, 7, 8, 9, 10, 11]. The stator of that motor has since been fully assembled and tested, the results of which are presented here.

When operating as a generator, a PMSM works by rotating permanent magnets near coils on the stator. The changing magnetic field induces voltage on those coils, known as back-EMF. That back-EMF induces current to flow through the coils when the circuit is completed. For a three-phase machine, such as the one being studied here, the stator has a multiple of three windings which are spaced such that the back-EMFs form a balanced three-phase set. Chapter 2 discusses back-EMF measurements using two different rotors on the same stator.

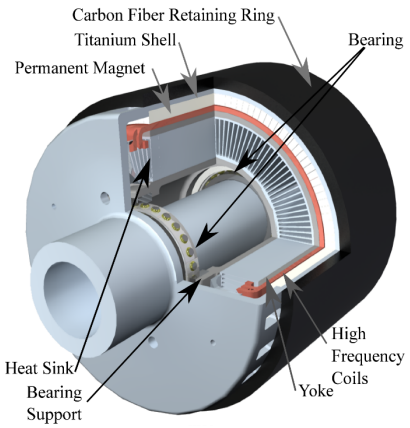

Figure 1.1: Labeled cutaway diagram of the full motor as designed.

In a machine that has more than one set of windings, how to connect the windings is an important design decision. For this machine, the design plan was to connect pairs of windings in parallel. Such a parallel connection means there is the possibility for circulating currents between the parallel windings. Measurements of these circulating currents are discussed in chapter 3.

Finally, work on selecting appropriate components for a motor testbed is discussed in chapter 4. Important tradeoffs between flexibility and complexity are discussed.

CHAPTER 2

BACK-EMF MEASUREMENTS

2.1 Stator Design

The two primary goals in designing this stator were to minimize weight and losses while delivering 1 MW of power. To reduce weight, stator teeth were eliminated and only a thin back iron was used. The elimination of stator teeth poses several manufacturing challenges. In slotted motors, it is common to wind the coils directly onto the teeth. Without slots, the coils must be form-wound separately and then mounted to the surface. The winding and placement on the surface both present opportunities for deviations from nominal dimensions and positions.

In the literature, there is increasing interest in slotless motor designs, often motivated by low weight. Analytical approaches to modeling these machines are presented and validated in [12, 13]. Another potential advantage of slotless stators is low cogging torque, due to nearly constant flux linkage at all rotor positions [14].

Some prototype motors with requirements similar to those of this project are described in the literature. In particular, there is a series of papers about a 640 kW machine designed for 10,000 rpm operation using Halbach array permanent magnet rotor and a slotless stator [15, 16, 17]. In [17] the authors acknowledge the risk of circulating currents described in chapter 3 of this thesis. They also describe problems with incorrect magnet orientations in the Halbach array, similar to issues described later in this chapter. In these papers, the manufacturing of the slotless stator is not described in detail.

Another completed prototype machine with a slotless radial flux stator is presented in [14], though few manufacturing and testing details are provided. In [18] the design of a limited rotation slotless machine is presented. Many other slotless machines in the literature are based on axial flux paths, often

featuring rotors on each side of the stator [19, 20, 21]. Design and manufacturing for that type of machine is very different from that for radial-flux slotless machines.

For the machine described here, the coils were form-wound by hand with dimensional tolerances of ±0.005 inches. A summary of important parameters is in Table 2.1. A more complete description of the stator can be found in [3, 9, 10]. Fig. 2.1 shows a photo of the final stator.

Table 2.1: Stator Description

Parameter	***Quantity***	***Unit***
Coil Active Length	9.5 (phase A) 10.25 (phase B) 11 (phase C)	inches
Pole Pairs	10	-
Phases	3	-
Design weight	36.6	kg
Actual weight	37.6	kg
Rated phase current	93	Arms
Rated total current	930	Arms
Rated line voltage	650	Vrms

2.2 Rotor Design

The rotor design features 10 magnetic pole pairs with magnets oriented in a Halbach array. This design has previously been mechanically validated up to 20% overspeed in [5]. As mentioned above, the machine was designed with an outer rotor. This allows a magnet containment ring without increasing the air gap. The manufacturing and installation of the magnets was significantly delayed and so we built an alternate, derated rotor in-house to allow for stator validation. Results of those tests are described in section 2.3. A comparison of that derated rotor and the final rotor is in Table 2.2. Once the final rotor was completed, we found that the magnets were installed incorrectly and conducted additional tests, as described in section 2.4.

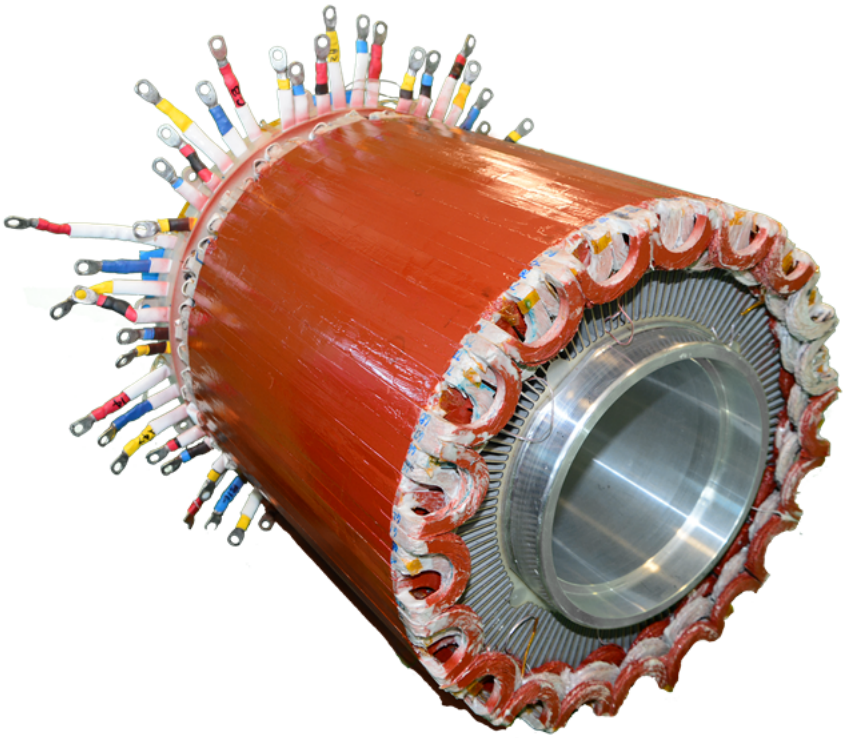

Figure 2.1: Final constructed stator.

Table 2.2: Rotor Description

Parameter	***Final Rotor***	***Derated Rotor***	***Unit***
Mechanical Air Gap	1.7	2	mm
Magnetic Air Gap	1.7	12.8	mm
Magnet Material	N45UH	N42	-
Magnet Thickness	0.485	0.25	in
Magnetization Direction	Halbach Array	Radial	-
Magnet Active Length	9.5	9	in
Pole Paris	10	10	-
Weight	41.5		kg
Back Iron Thickness	0	0.125	in

(a) Partially built with magnets attached but no back iron

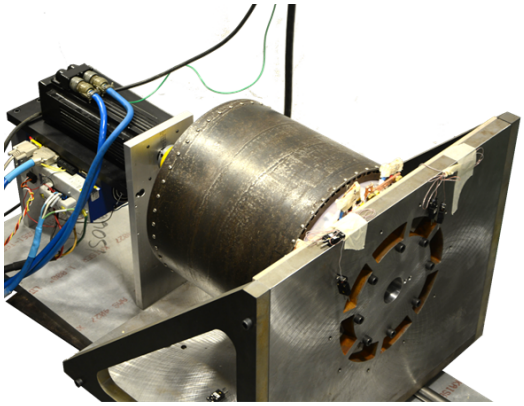

(b) Fully built and mounted on test stand.

Figure 2.2: Alternate rotor construction and test stand.

2.3 Derated Rotor Results

2.3.1 Derated Rotor Build

Since magnet installation on the full rotor was delayed, we decided to make a significantly derated rotor to allow for initial validation of stator performance at reduced power. This rotor was made primarily of Bakelite and built in-house. We designed this rotor to allow for quick and relatively low-cost manufacturing. Fig. 2.2 shows a photo of the rotor with the magnets in place but without the back iron attached, and the completed rotor on the test stand.

Each difference between the full-size rotor and alternate rotor results in the alternate rotor generating weaker magnetic fields on the windings and therefore smaller back-EMF generated by the windings. In addition, this rotor was not carefully balanced, so imbalance induced vibration made it unsafe to spin above a few hundred rpm. We built a two-dimensional finite element model to predict the expected performance of the stator when exposed to these magnetic fields.

2.3.2 Derated Rotor Back-EMF

First, we measured the back-EMF generated on each winding at 300 rpm. The phase-to-phase back-EMF waveform is shown in Fig. 2.3 with the FEA

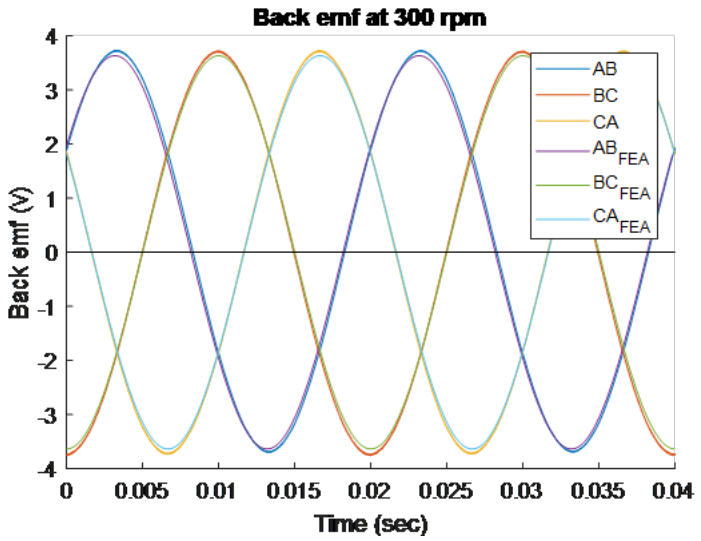

Figure 2.3: Back-EMF generated by one three-phase winding set at 300 rpm with derated rotor.

predicted waveform also shown. The measured line-line back-EMF waveform is nearly identical to the FEA prediction, both having less than 1% THD. The measured rms value is between 2.3% and 4.4% higher than predicted, distributed as shown in Fig. 2.4. The two-dimensional FEA assumes that the magnets and windings are of the same axial length; however the actual windings are axially longer than the magnets which contributes to higher back-EMF than predicted. Notably, the phase with longest active lengths (phase B-C line-line) has the highest back-EMF while the set with shortest active lengths (phase A-B line-line) has the lowest back-EMF.

Besides variation in back-EMF between the phases we observed variation between different winding sets of each phase. The ten winding sets are physically distributed around the circumference of the stator, with winding set 10 arbitrarily assigned to the top as shown in Fig. 2.5. A static eccentricity, where the center of the rotor and stator are not perfectly aligned, results in the magnets being closer to the windings on one side of the motor than the other side, driving different magnitudes of back-EMF. In fact, we observe that the back-EMF magnitude varies as a function of rotor position as shown in Fig. 2.5. We modified our finite-element model to include static eccentricity and found that the observed 1.5% variation in back-EMF magnitude is consistent with the axes of the rotor and stator being separated by 1.1 mm. Part of this static eccentricity is likely caused by manufacturing inaccuracies

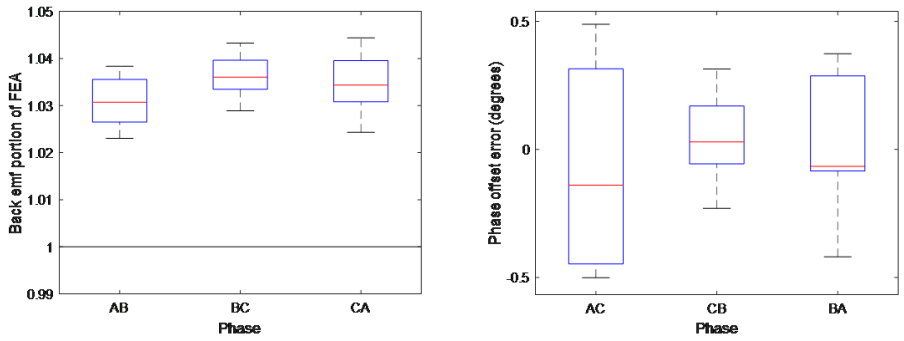

(a) Back-EMF magnitude error. (b) Back-EMF phase offset error.

Figure 2.4: Distribution of back-EMF errors generated by the 10 winding sets with derated rotor. Results are separated by line-line combination. Magnitude is normalized by the FEA predicted back-EMF.

of the derated rotor and the modified bearing arrangement used to mount it.

In addition to variation in the back-EMF magnitude, we observed slight phase offsets between windings of the same phase. In a perfect set of three-phase windings, there should be exactly 120 electrical degrees offset between the windings. Since our stator lacks winding slots, there is the possibility that windings were not perfectly spaced circumferentially causing some phase error. In fact, we found that within each three-phase set, no two voltages were more than ± 0.5 electrical degrees from the designed phase offset as summarized in Fig. 2.4. The largest phase errors were between phase A and phase C, which were the first and last ones to be attached to the stator. There is no correlation between this phase error and the circumference position on the stator.

On an ideal stator, there should be no time offset between windings of the same phase. In fact, our measurements show phase deviation of ± 1.75 electrical degrees between windings of the same phase. As shown in Fig 2.5, the circumferential position of these back-EMF phase variations follows a pattern similar to what we observed for the magnitude. Our finite-element model shows that this level of phase deviation is consistent with a static eccentricity of 4.5 mm, which is greater than the mechanical airgap implying that some other mechanism is at play.

It is well documented that static eccentricity can generate uneven magnetic pull, noise, and torque ripple and can be used for diagnostics [22],

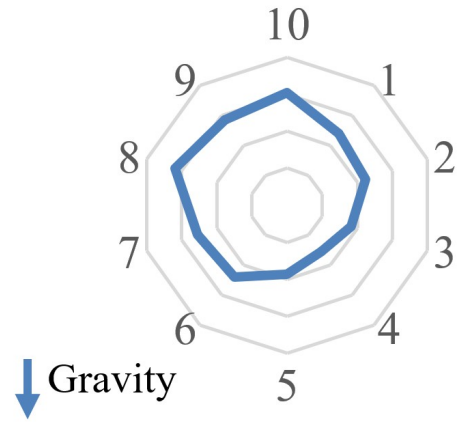

(a) Back-EMF magnitude vs mechanical position

Winding	A	B	C	Avg
1	1.120	1.117	1.121	1.119
2	1.118	1.120	1.121	1.120
3	1.119	1.122	1.127	1.123
4	1.120	1.124	1.127	1.124
5	1.125	1.129	1.130	1.128
6	1.122	1.125	1.129	1.125
7	1.122	1.126	1.130	1.126
8	1.121	1.122	1.125	1.122
9	1.121	1.122	1.127	1.123
10	1.115	1.119	1.120	1.118

(b) Back-EMF magnitude table

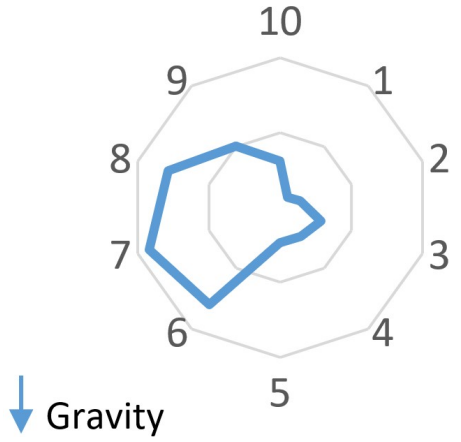

(c) Back-EMF phase vs mechanical position

Winding	A	B	C	Avg
1	-2.01	-1.59	-3.53	-2.38
2	-1.95	-1.73	-1.36	-1.68
3	-1.44	-1.15	-0.38	-0.99
4	-0.82	-0.99	-0.58	-0.80
5	1.66	1.79	1.77	1.74
6	1.91	2.22	2.94	2.36
7	2.62	2.78	2.98	2.79
8	1.13	1.50	2.44	1.69
9	-0.14	0.00	-1.87	-0.67
10	-0.96	-2.83	-2.41	-2.07

(d) Back-EMF phase table

Figure 2.5: Back-EMF magnitude and phase from derated rotor. Magnitude is normalized by FEA simulation.

[23]; however the phase offset between windings has not previously been well documented.

2.4 Full-Size Rotor Tests

2.4.1 Magnet Characterization

After magnet installation in the full-size rotor was completed, we measured the resulting magnetic field profile and determined that it does not match what is expected from a Halbach array as shown in Fig. 2.6. Two problems with the pattern became clear. First, the generated field is not sinusoidally varying, with most poles showing a consistent pattern. Second, some poles are different from the rest. Specifically, one of the 10 south poles is stronger than the rest in two of the three axial segments. Also, one north pole is stronger than the rest in one of the three axial segments. Using a finite element model we determined that a field with this profile can be created by horizontally reversing some of the magnets in the Halbach array as shown in Fig. 2.7.

2.4.2 Back-EMF Measurements

Although it is clearly far from ideal to have this distorted field profile since the magnitude of the projected field is reduced, the finite element model shows that if all 10 pole pairs are identical, the back-EMF generated has very low harmonic distortion and no harmonic contribution below the 9th harmonic. However, the one pole per revolution which is different than the rest does cause a periodic deviation in back-EMF. This conclusion is verified by the experimental waveforms shown in Fig. 2.8.

Fig. 2.9 shows the magnitude and phase offset error of the back-EMF generated by the full-size rotor. On average, the back-EMF magnitude is 12% higher than predicted in FEA, a larger increase than seen in the derated rotor. The larger deviation for this full-size rotor than for the derated rotor can be explained by the fact that the magnetic airgap is much smaller and the magnets are much thicker so the end-windings play a larger role. Unfortunately, the phase offset error is also larger for this rotor than the derated

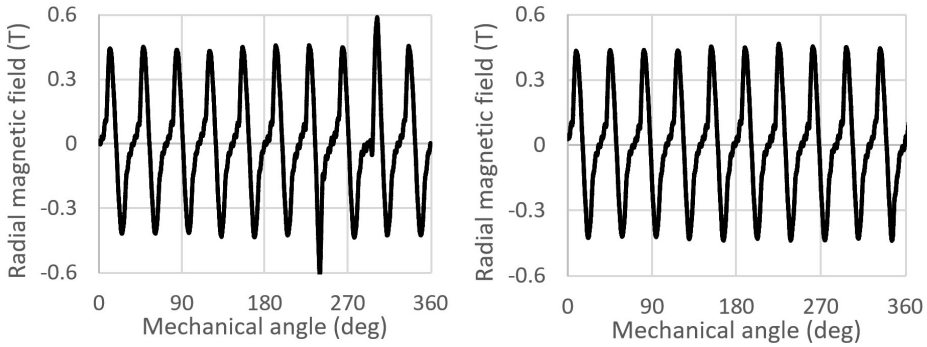

(a) Segment closest to heatsink inlet

(b) Middle segment

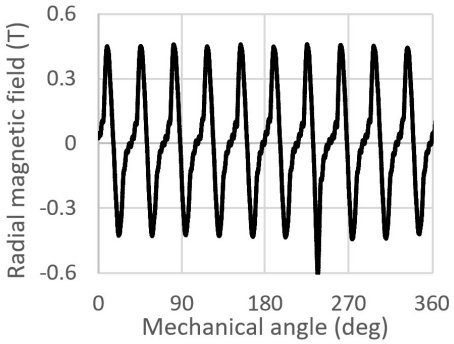

(c) Segment closest to fan

Figure 2.6: Magnetic field strength around the circumference of the rotor measured at the axial center of each of the three magnet segments. Note that not all poles are the same shape.

(a) Magnet orientations of one pole pair as designed for Halbach array.

(b) Magnet orientations of one pole pair as modeled for FEA to match delivered rotor. Arrows shown in red are those that differ from the design

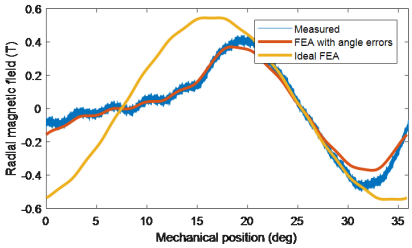

(c) Magnetic field strength as a function of position for one representative pole pair showing designed, measured, and FEA.

Figure 2.7: Designed and manufactured magnet orientations.

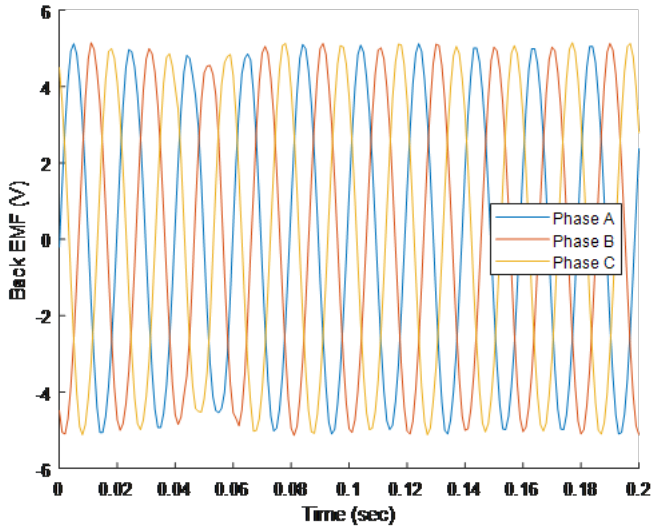

Figure 2.8: Back-EMF of one three-phase set for one complete mechanical rotation at 300 rpm of full-size rotor.

rotor.

Fig. 2.10 shows the back-EMF magnitude and phase variation as a function of winding position on the stator. For the full-size rotor there is about half the variation in back-EMF magnitude as for the derated rotor implying a smaller static eccentricity. However, the phase deviation is larger for this rotor than the derated rotor.

2.4.3 Loss Power Measurements

Loss modeling is a significant challenge in motor design. Since the performance of this motor is thermally limited, loss model errors can have significant impacts on achievable power densities. We sought to validate our loss models by spinning the motor in an open-circuit configuration. Fig. 2.11 shows the loss power as a function of speed. These losses include windage, fan pumping, hysteresis and eddy current iron, and ac copper losses. These results are consistent with prior loss models and preliminary results of ongoing experiments. Thorough loss measurements and analysis will be conducted on the final rotor once it is rebuilt with correct magnet orientations and will be reported in a future publication.

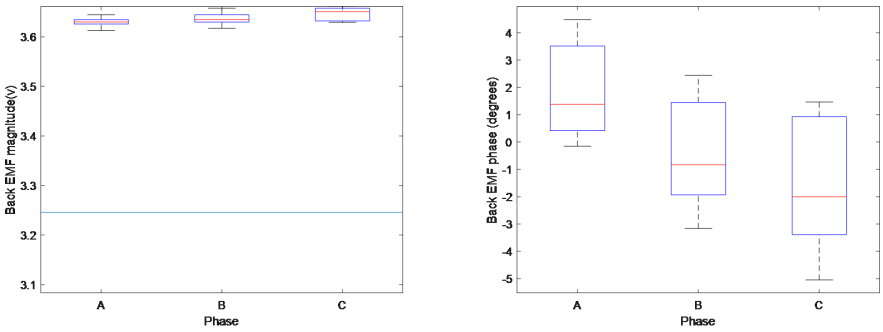

(a) Back-EMF magnitude error. (b) Back-EMF phase offset error.

Figure 2.9: Distribution of back-EMF errors generated by the 10 winding sets with full-size rotor at 302 rpm. Results are separated by line-line combination. Magnitude is normalized by the FEA predicted back-EMF.

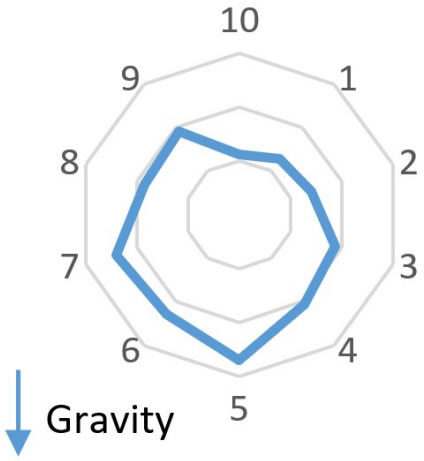

(a) Back-EMF magnitude vs mechanical position

Phase back-emf magnitude

Winding	A	B	C	Avg
1	1.120	1.117	1.121	1.119
2	1.118	1.120	1.121	1.120
3	1.119	1.122	1.127	1.123
4	1.120	1.124	1.127	1.124
5	1.125	1.129	1.130	1.128
6	1.122	1.125	1.129	1.125
7	1.122	1.126	1.130	1.126
8	1.121	1.122	1.125	1.122
9	1.121	1.122	1.127	1.123
10	1.115	1.119	1.120	1.118

(b) Back-EMF magnitude table

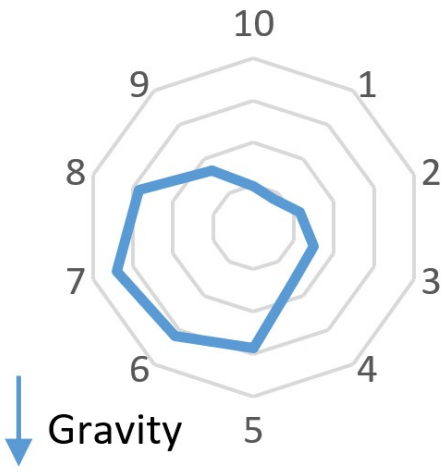

(c) Back-EMF phase vs mechanical position

Phase deviation (electrical degrees)

Winding	A	B	C	Avg
1	-2.01	-1.59	-3.53	-2.38
2	-1.95	-1.73	-1.36	-1.68
3	-1.44	-1.15	-0.38	-0.99
4	-0.82	-0.99	-0.58	-0.80
5	1.66	1.79	1.77	1.74
6	1.91	2.22	2.94	2.36
7	2.62	2.78	2.98	2.79
8	1.13	1.50	2.44	1.69
9	-0.14	0.00	-1.87	-0.67
10	-0.96	-2.83	-2.41	-2.07

(d) Back-EMF phase table

Figure 2.10: Back-EMF magnitude and phase from full-size rotor. Magnitude is normalized by FEA simulation.

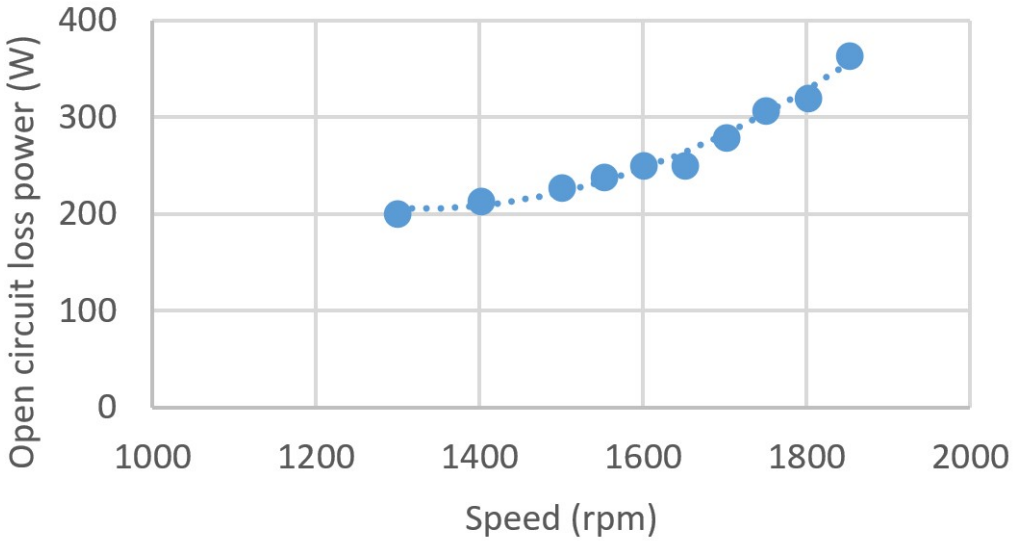

Figure 2.11: Open-circuit loss power as function of rotor speed.

CHAPTER 3

CIRCULATING CURRENT MEASUREMENTS

The stator is built with 10 sets of three-phase windings physically separated around the circumference. The original design intent is that five three-phase inverters will each drive a pair of these windings connected in parallel. With parallel windings, any impedance or back-EMF imbalance could drive circulating currents in the parallel windings and as well as voltages between the neutral points if they are left floating.

3.1 Derated Rotor

When testing the derated rotor, we left the neutral points floating and connected five pairs of windings in parallel as intended for the final drive system; see the circuit diagram in Fig. 3.1. We then measured the voltages between the neutral points of paralleled windings. The largest harmonic component of these voltages was the same frequency and in phase with the phase A back-EMF. There were also significant third harmonics. The rms magnitude of the neutral-point voltages was between 0.35% and 0.71% of the line-line rms back-EMF. On the final machine, this percent of line-line voltage scales to 4.6 V at full speed.

3.2 Full-Size Rotor

With the full-size rotor, we connected all 10 winding sets in parallel to test the worst-case scenario for circulating currents as shown in Fig. 3.2. With the neutral points left floating relative to ground and each other, the circulating currents through each phase winding peaked at 12.2 A when operating at 300 rpm. Assuming it scales linearly, this would lead to a peak of 610 A at full rated speed. Such high current spikes would cause increased dc and ac

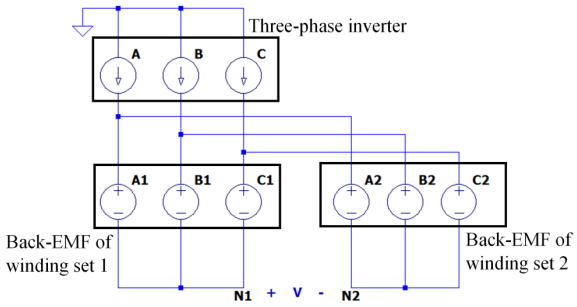

Figure 3.1: Circuit diagram of a pair of parallel winding sets connected in parallel.

losses in the wire as well as projecting a field into the magnets, generating eddy current losses.

When we connected all 10 neutral points together, the peak phase current was 11.4 A and the maximum current through a neutral wire was 4.48 A. The highest circulating currents on a given channel occur when the magnetic pole with higher flux passes that pole. That current must then be balanced out by the other windings resulting in negative currents in most other phases.

Passing the currents through the Fourier transform, we can see the strongest harmonic component is at the fundamental electrical frequency. The third harmonic is also present. The third harmonic corresponds to the stronger pole passing over a different winding elsewhere on the machine.

With the neutral points connected together there are currents from each winding through the neutral connection. The strongest component for that current is the third harmonic, again corresponding to the stronger pole passing over a winding somewhere on the machine. Together, these large circulating currents at low speeds highlight the importance of correct magnet placement and matched back-EMFs between windings with parallel winding connections.

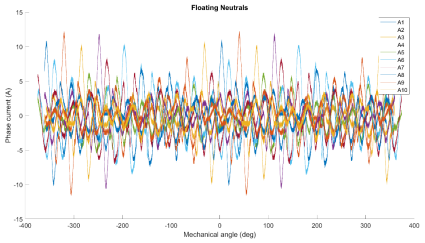

(a) Phase current waveforms when neutral points are left floating

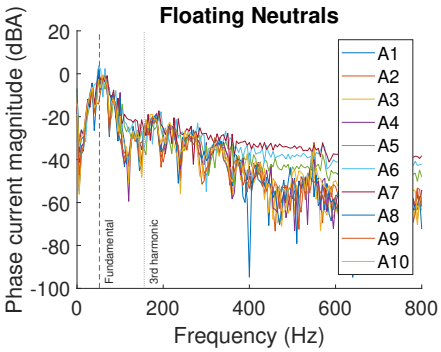

(b) Phase current spectrum when neutral points are left floating

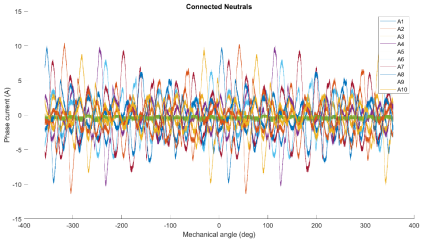

(c) Phase current waveforms when neutral points are connected

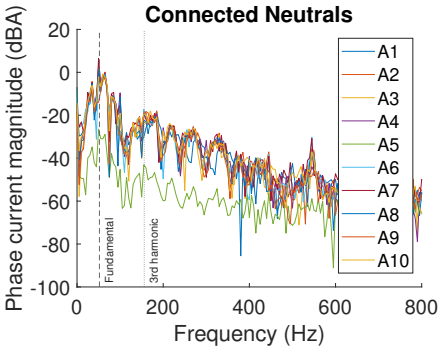

(d) Phase current spectrum when neutral points are connected

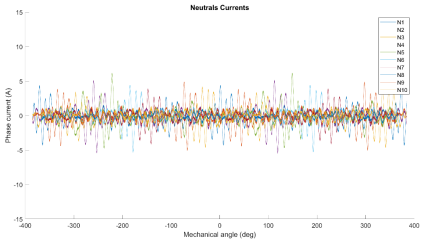

(e) Current waveforms through the neutral wires with all 10 connected

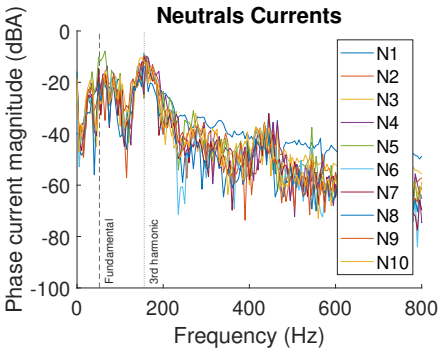

(f) Current spectrum through the neutral wires with all 10 connected

Figure 3.2: Circulating currents with all 10 winding sets connected in parallel.

CHAPTER 4

TEST BED DEVELOPMENT

4.1 Winding Configurations

This motor consists of 10 sets of three-phase windings. Both ends of each winding are brought out of the motor as leads, which means there are 60 total connections available. Having all the connections available makes this motor highly reconfigurable, allowing for flexible test configurations. For the initial phase testing this machine, we want to operate it as a generator driving a resistive load.

The conceptually simplest approach would be to attach a resistor directly to each winding as shown in Fig. 4.1. In this configuration, each winding is entirely independent; however this would require 60 connections, at least 30 resistors, and sensors to detect voltage and current from each winding.

The number of external connections can be cut in half by connecting the machine windings in three-phase sets as shown in Fig. 4.2, but still requires the same number of resistors. This connection could be in delta or wye, but wye configuration was chosen since the mechanical placement of windings

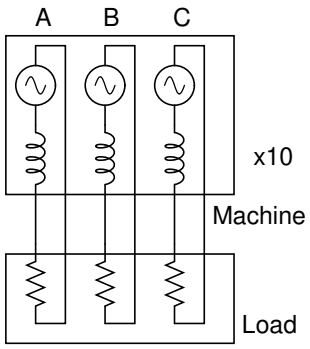

Figure 4.1: Circuit diagram for direct connection from each winding to a resistor.

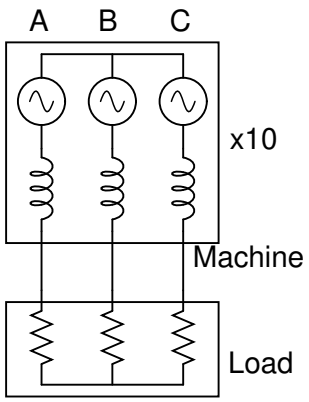

Figure 4.2: Circuit diagram for windings and resistors in wye configuration.

is better suited to that. With this configuration, net current in each three-phase set is zero; therefore two current sensors per phase are sufficient to fully instrument the machine.

To further reduce the number of components required, windings could be connected in series or parallel, as shown in Fig. 4.3. With series windings, the back-EMFs of each connected winding are added together resulting in higher voltages at the load. The currents through each set of series windings are equal.

With parallel windings, the voltages across each winding are made equal by the connecting wire. This means that if the back-EMFs generated by each connected winding are not exactly equal, the voltages across the winding equivalent impedances will be unequal. In turn, these voltages will generate unequal currents in each winding resulting in a circulating current loop. This circulating current does not contribute to torque generation but does add to losses. Similarly if the back-EMFs generated in each parallel winding are equal but the impedances differ, circulating currents will also be generated.

Fig. 4.3 shows five pairs of windings connected together. With this motor, there are many possible series/parallel combinations, including ones where parallel groups of windings are connected in series or vice versa.

4.2 Resistor Selection

The tests described in chapter 2 took place on a dynamometer on campus. Since that testing, a new research facility from the POETS center was con-

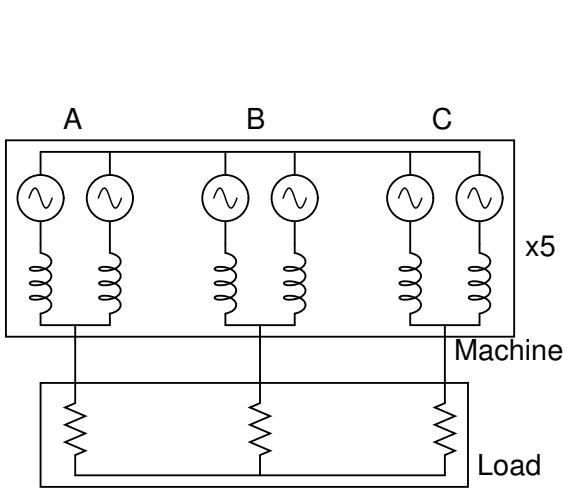

(a) Parallel connection

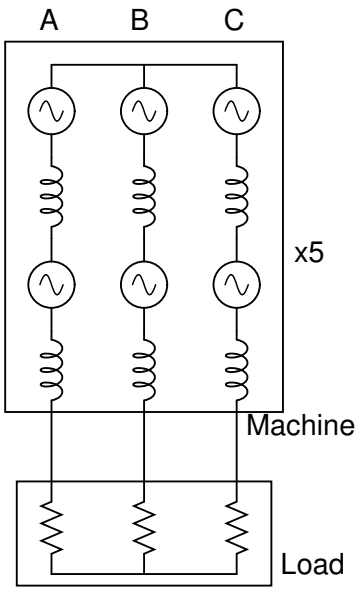

(b) Series connection

Figure 4.3: Series and parallel winding connections.

structed with a much larger dynamometer. This building has maximum power capacity of 166 kW and is currently limited to 6000 rpm. This dynamometer will allow us to operate the machine as a generator to drive resistive loads.

Ideally we would like to be able to connect the machine to a resistive load that can be configured to explore the full range of speeds and torques with the fewest total resistors necessary. The full power/speed range of the machine as designed compared to the range achievable at POETS is shown in Fig. 4.4.

The minimum number of resistors required to evenly load the whole machine is three times the number of winding groups as determined by the series/parallel connections of the windings. So if there are five sets of two windings connected in series or parallel, at least 15 resistors are required. Of course, the resistors themselves can also be connected in series or parallel combinations allowing for far more flexibility.

High-power resistors are available in a variety of power ratings and resistances. The most common power ratings are 1 kW and 2.5 kW. Available resistances include 1 Ω, 4.7 Ω, and 10 Ω. A MATLAB script was developed to select the type of resistor that provided the best coverage of the test space. As an input the script takes the number of resistors, power rating,

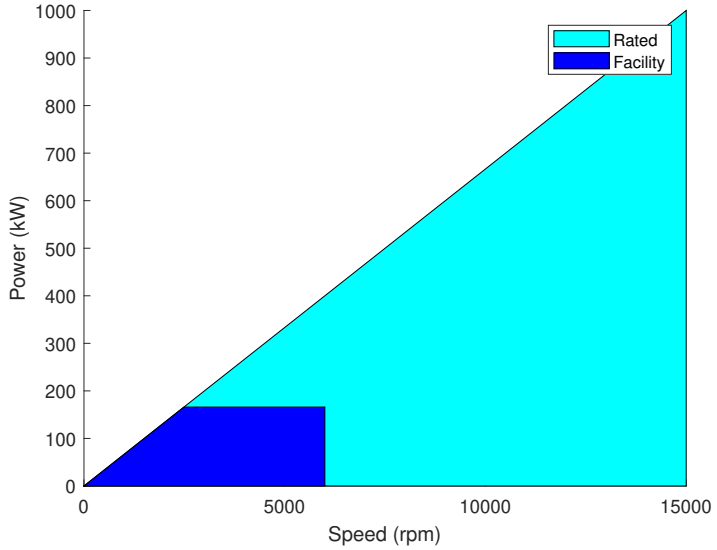

Figure 4.4: Machine and facility power range.

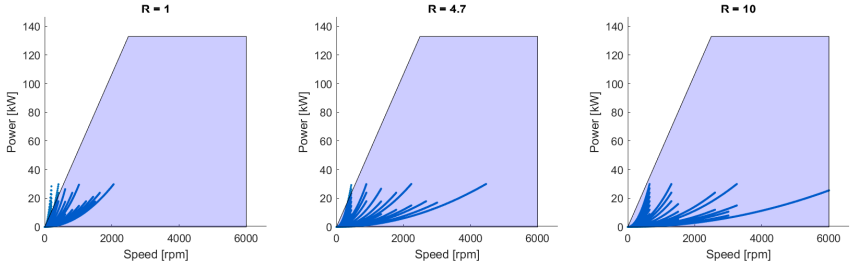

Figure 4.5: Achievable test cases with 30, 1 kW resistors and no windings in parallel.

and resistance. It then calculates what series/parallel combinations of both resistors and windings are feasible. Then using all the possible combinations, it calculates the output power at each speed.

With 30 resistors rated at 1 kW each and none of the windings in parallel, the achievable test cases are shown in Fig. 4.5. Without any winding parallel connections, the 1 Ω resistors are only able to cover a small part of the range while both 4.7 Ω and 10 Ω resistors provide better coverage. Allowing windings to be connected in parallel, the achievable cases are shown in Fig. 4.6. As expected, opening up more winding configurations allows for a wider range of test cases.

If we consider the same total rated power capacity of 75 kW, that could be achieved with 30, 2.5 kW resistors or with 75, 1 kW resistors. Fig. 4.7 shows the test cases covered in each of these cases. As expected, more total

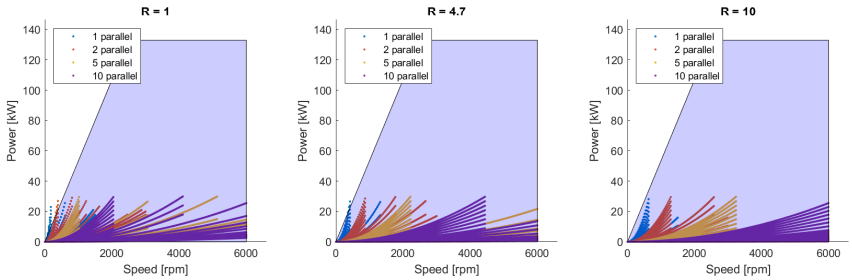

Figure 4.6: Achievable test cases with 30, 1 kW resistors with windings in parallel.

resistors allows for greater flexibility. The disadvantage of using a large number of lower rated resistors is that building racks to hold them quickly becomes complicated and expensive. The possible test cases using 30, 2.5 kW resistors and no windings in parallel are shown in Fig. 4.8. In this case, the 10 Ω resistors provide better coverage of the space without having the risk of circulating currents.

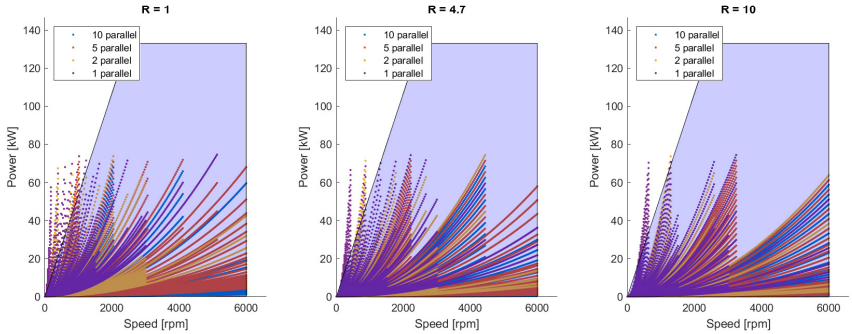

(a) 75, 1 kW resistors

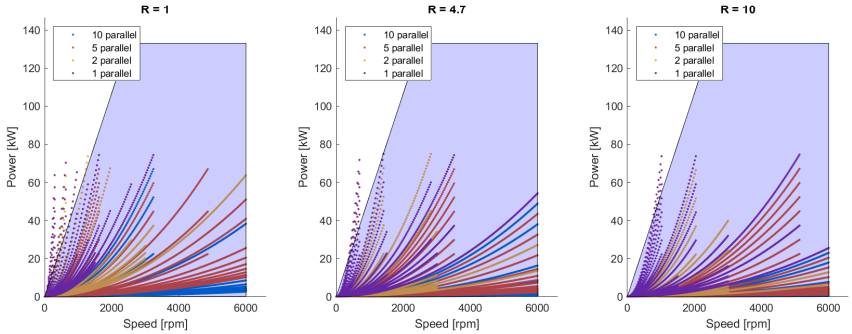

(b) 30, 2.5 kW resistors

Figure 4.7: Achievable test cases with fixed combined resistor power rating of 75 kW.

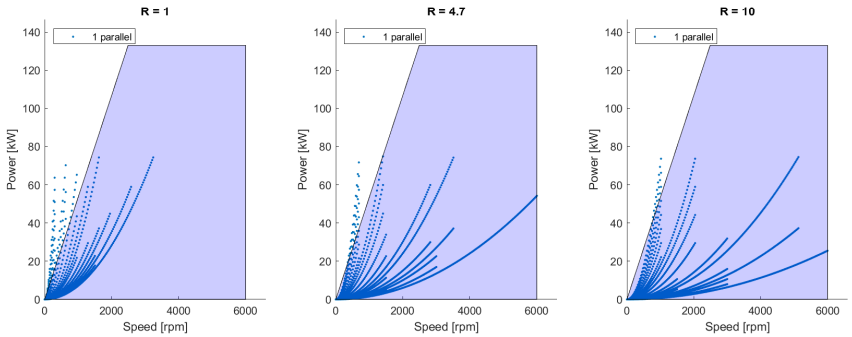

Figure 4.8: Achievable test cases with 30, 2.5 kW resistors and no windings connected in parallel.

CHAPTER 5

CONCLUSION

We have demonstrated that it is possible to build a slotless stator with litz wire windings with tight manufacturing tolerances. Through testing with two different rotors, we have demonstrated that this stator produces back-EMF on all 10 sets of three-phase windings. The magnitudes and phases of these back-EMFs are closely correlated to those predicted by FEA. Back-EMF or impedance mismatches between winding sets have the potential to introduce significant circulating currents. Careful rotor manufacturing is vital to avoid defects and inconsistencies in the applied magnetic field. Minimizing static eccentricity is also important for maintaining consistent back-EMF during each rotation. These promising test results indicate that this motor may be an enabling technology for further aircraft propulsion electrification.

The full-sized rotor is currently being rebuilt with corrected magnet alignment. Once that rebuild is complete, it will be tested using the testbed with resistors selected for great flexibility while maintaining a reasonable part count.

REFERENCES

[1] R. Jansen, C. Bowman, A. Jankovsky, R. Dyson, and J. Felder, "Overview of NASA electrified aircraft propulsion (EAP) research for large subsonic transports," in *53rd AIAA/SAE/ASEE Joint Propulsion Conference*. American Institute of Aeronautics and Astronautics, July 2017. [Online]. Available: https://arc.aiaa.org/doi/10.2514/6.2017-4701

[2] R. Jansen, G. V. Brown, J. L. Felder, and K. P. Duffy, "Turboelectric aircraft drive key performance parameters and functional requirements," in *51st AIAA/SAE/ASEE Joint Propulsion Conference*. American Institute of Aeronautics and Astronautics, July 2015. [Online]. Available: http://arc.aiaa.org/doi/10.2514/6.2015-3890

[3] A. Yoon, X. Yi, J. Martin, Y. Chen, and K. Haran, "A high-speed, high-frequency, air-core PM machine for aircraft application," in *2016 IEEE Power and Energy Conference at Illinois (PECI)*, Feb. 2016, pp. 1–4.

[4] A. D. Anderson, Y. Wang, Y. Yu, and K. S. Haran, "Experimental validation of a high-power slotless stator," in *2019 IEEE International Electric Machines & Drives Conference (IEMDC)*. San Diego, CA, USA: IEEE, May 2019. [Online]. Available: https://ieeexplore.ieee.org/document/8785264/ pp. 1564–1569.

[5] R. Sanchez, A. Yoon, X. Yi, L. Zheng, Y. Chen, K. S. Haran, A. Provenza, and J. Veres, "Mechanical validation of a high power density external cantilevered rotor," *IEEE Transactions on Industry Applications*, vol. 54, no. 4, pp. 3208–3216, July 2018.

[6] X. Yi, R. Sanchez, K. Haran, J. Veres, A. T. Perry, and P. J. Ansell, "Self-pumped air-cooling design for a high-speed high-specific-power motor," in *2018 IEEE Transportation Electrification Conference and Expo (ITEC)*, June 2018, pp. 274–279.

[7] Y. Chen, R. Sanchez, A. Yoon, and K. S. Haran, "Mechanical design considerations of an "ironless," high-specific-power electric machine," *IEEE Transactions on Transportation Electrification*, vol. 3, no. 4, pp. 855–863, Dec. 2017. [Online]. Available: http://ieeexplore.ieee.org/document/7997807/

[8] X. Yi, A. Yoon, and K. S. Haran, "Multi-physics optimization for high-frequency air-core permanent-magnet motor of aircraft application," in *2017 IEEE International Electric Machines and Drives Conference (IEMDC)*. Miami, FL, USA: IEEE, May 2017. [Online]. Available: http://ieeexplore.ieee.org/document/8002293/ pp. 1–8.

[9] N. J. Renner, J. D. Lenz, X. Yi, and K. S. Haran, "Development of form-wound air-core armature windings for high-frequency electric machines," in *2017 IEEE International Electric Machines and Drives Conference (IEMDC)*. Miami, FL, USA: IEEE, May 2017. [Online]. Available: http://ieeexplore.ieee.org/document/8002268/ pp. 1–8.

[10] J. D. Lenz, N. J. Renner, X. Yi, and K. S. Haran, "Insulation considerations in form-wound armature windings for high-frequency electric machines," in *2018 IEEE Power & Energy Society General Meeting (PESGM)*. Portland, OR: IEEE, Aug. 2018. [Online]. Available: https://ieeexplore.ieee.org/document/8586101/ pp. 1–5.

[11] J. Martin, A. Yoon, A. Jin, and K. S. Haran, "High-frequency litz "air-gap" windings for high-power density electrical machines," *Electric Power Components and Systems*, vol. 45, no. 7, pp. 798–805, Apr. 2017. [Online]. Available: https://www.tandfonline.com/doi/full/10.1080/15325008.2017.1310951

[12] A. Tessarolo, L. Branz, and C. Bruzzese, "A compact analytical expression for the load torque in surface permanent-magnet machines with slotless stator design," in *2013 IEEE Workshop on Electrical Machines Design, Control and Diagnosis (WEMDCD)*. Paris: IEEE, Mar. 2013. [Online]. Available: http://ieeexplore.ieee.org/document/6525160/ pp. 8–17.

[13] A. Chebak, P. Viarouge, and J. Cros, "Improved analytical model for predicting the magnetic field distribution in high-speed slotless permanent-magnet machines," *IEEE Transactions on Magnetics*, vol. 51, no. 3, pp. 1–4, Mar. 2015. [Online]. Available: http://ieeexplore.ieee.org/document/7093422/

[14] M.-M. Koo, J.-Y. Choi, J.-H. Jeong, H.-J. Shin, and K. Hong, "Characteristic analysis of permanent-magnet synchronous generator with slotless stator structure considering magnetic/mechanical air gap using semi-3-D analytical method," *IEEE Transactions on Magnetics*, vol. 51, no. 11, pp. 1–4, Nov. 2015. [Online]. Available: http://ieeexplore.ieee.org/document/7119585/

[15] F. Luise, A. Tessarolo, S. Pieri, P. Raffin, M. Di Chiara, F. Agnolet, and M. Scalabrin, "Design and technology solutions for high-efficiency high-speed motors," in *2012 XXth International Conference on Electrical Machines*. Marseille, France: IEEE, Sep. 2012. [Online]. Available: http://ieeexplore.ieee.org/document/6349857/ pp. 157–163.

[16] F. Luise, A. Tessarolo, F. Agnolet, S. Pieri, M. Scalabrin, and P. Raffin, "A high-performance 640-kW 10.000-rpm Halbach-array PM slotless motor with active magnetic bearings. Part I: Preliminary and detailed design," in *2014 International Symposium on Power Electronics, Electrical Drives, Automation and Motion*. Ischia, Italy: IEEE, June 2014. [Online]. Available: http://ieeexplore.ieee.org/document/6871944/ pp. 1237–1244.

[17] F. Luise, A. Tessarolo, F. Agnolet, S. Pieri, M. Scalabrin, and P. Raffin, "A high-performance 640-kW 10.000-rpm Halbach-array PM slotless motor with active magnetic bearings. Part II: Manufacturing and testing," in *2014 International Symposium on Power Electronics, Electrical Drives, Automation and Motion*. Ischia, Italy: IEEE, June 2014. [Online]. Available: http://ieeexplore.ieee.org/document/6871945/ pp. 1245–1250.

[18] Z. Jibin, Y. Guodong, X. Yongxiang, C. Xia, L. Yong, and W. Qian, "Development of a slotless limited-angle torque motor for reaction wheels torque measurement system," *IEEE Transactions on Magnetics*, vol. 50, no. 11, pp. 1–4, Nov. 2014. [Online]. Available: http://ieeexplore.ieee.org/lpdocs/epic03/wrapper.htm?arnumber=6971385

[19] S.-Y. Sung, J.-H. Jeong, Y.-S. Park, J.-Y. Choi, and S.-M. Jang, "Improved analytical modeling of axial flux machine with a double-sided permanent magnet rotor and slotless stator based on an analytical method," *IEEE Transactions on Magnetics*, vol. 48, no. 11, pp. 2945–2948, Nov. 2012. [Online]. Available: http://ieeexplore.ieee.org/document/6332767/

[20] H.-J. Shin, J.-Y. Choi, Y.-S. Park, M.-M. Koo, S.-M. Jang, and H. Han, "Electromagnetic vibration analysis and measurements of double-sided axial-flux permanent magnet generator with slotless stator," *IEEE Transactions on Magnetics*, vol. 50, no. 11, pp. 1–4, Nov. 2014. [Online]. Available: http://ieeexplore.ieee.org/document/6971618/

[21] E. Mendrela, R. Beniak, and R. Wrobel, "Influence of stator structure on electromechanical parameters of torus-type brushless DC motor," *IEEE Transactions on Energy Conversion*, vol. 18, no. 2, pp. 231–237, June 2003. [Online]. Available: http://ieeexplore.ieee.org/document/1201094/

[22] D. Dorrell, Min-Fu Hsieh, and YouGuang Guo, "Unbalanced magnet pull in large brushless rare-earth permanent magnet motors with rotor eccentricity," *IEEE Transactions on Magnetics*, vol. 45, no. 10, pp. 4586–4589, Oct. 2009. [Online]. Available: http://ieeexplore.ieee.org/document/5257290/

[23] J. Cameron, W. Thomson, and A. Dow, "Vibration and current monitoring for detecting airgap eccentricity in large induction motors," *IEE Proceedings B Electric Power Applications*, vol. 133, no. 3, p. 155, 1986. [Online]. Available: https://digital-library.theiet.org/content/journals/10.1049/ip-b.1986.0022